Supporting Information for

Chitosan confined pyrolysis strategy enhances the catalytic performance of carbon material based on a novel carboxyl functionalization design MOF

Dongsheng Wang,[abc] Tingyu He,[ab] Mingyue Fan,[a] Tuotuo Li,[a] Haina Qi,[ac] Zihan Lin,[*a] Xiaoli Hu[*a] and Zhongmin Su[*a]

[a]School of Materials Science and Engineering, Changchun University of Science and Technology, Changchun 130022, China. Email: linzihan@cust.edu.cn; huxiaoli1113@cust.edu.cn; zmsu@nenu.edu.cn

[b]Changchun Technical University of Automobile, Changchun, 130013, China.

[c]School of Materials Science and Engineering, Jilin Jianzhu University, Changchun 130119, China.

Contents

1. Materials and measurements

The chemicals and solvents used in this chapter are commercially purchased, analytical grade, and can be used without further purification. $Co(NO_3)_2 \cdot 6H_2O$, 2,4,6-tri(4-pyridyl)-1,3,5-triazine (TPT), [1,1'-biphenyl]-3,4',5-tricarboxylic acid (bptc), 4-nitrophenol (4-NP), sodium borohydride ($NaBH_4$) and chitosan (CTS) (mol wt: 50,000-190,000 Da based on viscosity) were purchased from Energy Chemical. 1-ethyl-(3-dimethylaminopropyl) carbamide (EDC), n-hydroxysuccinimide (NHS) were derived from Macklin. N,N-dimethylacetamide (DMA) was supplied by Sigma-Aldrich.

Single crystal data were collected at room temperature on A Bruker Smart Apex II CCD X-ray diffractometer. Monochromatic Mo Kα radiation (λ=0.71073 A) of graphite monochromator was used as the incident light source. Crystal structure analysis was performed using SHElXTV-97 package. SADABS program was used to correct the data absorption. The morphology of the materials was observed by field emission scanning electron microscope (FE-SEM) and transmission electron microscopy (TEM). X-ray diffractometer (XRD) was used to study the crystal phase of the material with a scanning range of 5 °-80 ° and a scanning speed of 5 ° min^{-1}. The composition and chemical states of elements on the surface of the material were studied by X-ray photoelectron spectroscopy (XPS). Thermogravimetric analysis (TGA) was performed on the TA STD-Q600 thermal analyzer. The specific surface area of the material was calculated by Brunauer-Emmett-Teller (BET) method, and the pore size distribution was calculated by Barrett-Joyner-Halenda (BJH) model. Ultraviolet spectral data were obtained by Jasco V-770 spectrophotometer.

2. Synthesis and Methods

Synthesis of Co-MOF (-COOH). A mixture of TPT (20.8 mg, 0.07 mmol), bptc (28.6 mg, 0.1 mmol) and Co $(NO_3)_2 \cdot 6H_2O$ (29.1 mg, 0.1 mmol) was dissolved in a mixture of 2 mL DMA and 4 mL deionized water. Then the mixture was loaded into a 15 mL polytetrafluoroethylene high-pressure reactor and reacted under self-pressure in an oven at 100 ℃ for 3 days. After the reaction, the reactor is cooled naturally to room temperature to obtain brownish-yellow massive crystals. The obtained crystalline

products were washed three times with the mixed solution of DMA/water (v:v=1:2), filtered and dried at room temperature for standby. $C_{27}H_{22}N_4O_9Co$ element analysis calculation value (%): C, 45.92; H. 4.20; N. 14.61, measured value (%): C, 53.55; H. 3.64; N. 9.26. R (KBr, cm^{-1}): 440.21 (W), 715.32 (W), 1061.08 (W), 1444.59 (W), 1615.46 (W), 498.96 (m), 719.32 (m), 1061.08 (m), 1444.59 (m), 1615.46 (m), 640.46 (s), 785.82 (s), 1373.45 (s), 1514.59 (s), 1615.46 (s). CCDC-2102334 contains the supplementary crystallographic data of **Co-MOF (-COOH)**.

Synthesis of Co-MOF-*g*-CTS and Co-MOF/CTS. First, weigh 1000 mg of CTS and dissolve it in 200 ml of deionized water, add 0.5 % formic acid to adjust the pH of the solution between 3 and 4, heat and stir until CTS is completely dissolved, and then cool to room temperature for standby. Then take 10 mL of the above solution, add 30 mL of deionized water and 20 mL of DMA solution stir evenly, and then add 50 mg of **Co-MOF (-COOH)**, 20 mg of EDC, and 20 mg of NHS to the above-mixed solution with CTS respectively, stir at room temperature for 2 h, centrifuge the product after the reaction, and wash it with methanol for three times to obtain the Co-MOF-*g*-CTS material thought one-pot method. Co-MOF/CTS was obtained by mixing Co-MOF and CTS by physical grinding in a mortar according to the grafting rate of Co-MOF-*g*-CTS.

Synthesis of (P)-T catalyst.

Co-MOF (-COOH), Co-MOF-*g*-CTS and Co-MOF/CTS were placed in the alumina crucible, and then transferred to the tube furnace for heat treatment under N_2 atmosphere at a heat treatment temperature of 600 °C or 900 °C and a heating rate of 5 °C min^{-1}. After heat treatment, they were naturally cooled to room temperature. The obtained carbon-based material is denoted as (P)-T, where P represents the precursor of the material and T represents the pyrolysis temperature.

Catalytic reduction of 4-NP.

A The catalytic activity of carbon-based material (P)-T was monitored by UV-vis. The 4-NP catalytic reduction reaction was carried out in a quartz cuvette at room

temperature. First, 0.2 mL of 2.5 mM of 4-NP solution and 2.5 mL of deionized water were added to the quartz cuvette, and then 0.2 mL of 0.2 mM of newly prepared $NaBH_4$ solution was dropped. At this time, the solution changed from light yellow to bright yellow. Finally, 0.1 mL of a mixture of (P)-T uniformly dispersed in ultra-pure water with a concentration of 1 mg mL^{-1} was dropped. The absorbance of the solution in the cuvette was measured at different times, and the rate and process of the reduction reaction were monitored by recording the UV-vis spectra of the reaction system at different time intervals.

3. Characterizations and results

Table S1 Crystallographic data of **Co-MOF (-COOH)**.

Compound	Co-MOF (-COOH)
Empirical formula	$C_{27}H_{22}CoN_4O_9$
Formula weight	551.37
Temperature/K	296.15
Crystal system	trigonal
Space group	R-3
a/Å	26.746(16)
b/Å	26.746(16)
c/Å	20.833(12)
α/°	90
β/°	90
γ/°	120
Volume/$Å^3$	12906(17)
Z	18
F(000)	5058.0
2θ range for data collection/°	4.024 to 50
Index ranges	$-31 \leq h \leq 31$, $-25 \leq k \leq 31$, $-24 \leq l \leq 24$
Reflections collected	24753

Data/restraints/parameters	5043/0/344
Independent reflections	5043 [R_{int} = 0.0447, R_{sigma} = 0.0366]
Goodness-of-fit on F^2	1.045
Final R indexes [I>=2σ (I)]	R_1 = 0.0307, wR_2 = 0.0767
Final R indexes [all data]	R_1 = 0.0413, wR_2 = 0.0816

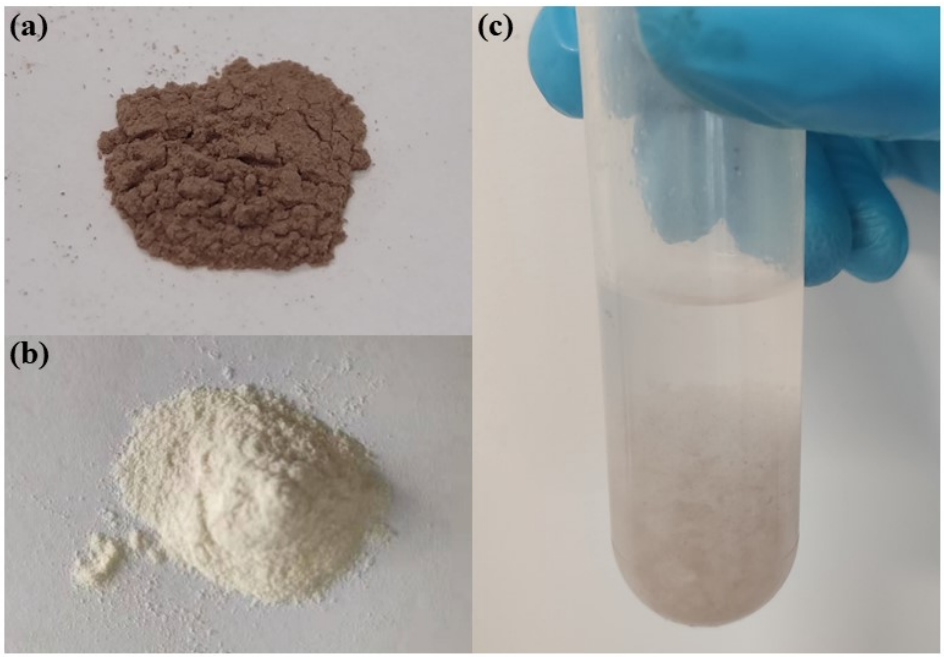

Fig. S1 Digital images of (a) **Co-MOF (-COOH)** and (b) CTS, (c) Digital picture of Co-MOF-*g*-CTS in methanol.

TEM was used to observe the particle dispersion and particle size of carbon-based nanomaterials prepared by different precursors. The internal details of the (P)-T material can be observed intuitively. During the pyrolysis process, the metal ions in the precursor are transformed into nanoparticles. The particles in (Co-MOF)-600 are evenly distributed in the carbon layer, and the particle size is between 12-39 nm (Fig. S2a). While the particles in (Co-MOF)-900 gather together to form larger particles (129-742 nm) and even overflow the carbon layer (Fig. S2b), which shows that low-temperature carbonization is easy to generate small particles.[1] The particles in (Co-MOF-*g*-CTS)-600 are protected by a layer of carbon shell, forming a core-shell structure, and the dispersion of particles is very uniform, with the particle size range

about 8-40 nm (Fig. S2c). It can be seen from Fig. S2d that the particles are also evenly dispersed in (Co-MOF-*g*-CTS)-900 and the particle size range is relatively concentrated (47-81 nm). Compared with (Co-MOF)-900, the particle dispersion and size of (Co-MOF-*g*-CTS)-900 are greatly improved at high-temperature carbonization, which indicates that the CTS confined pyrolysis strategy is conducive to the formation of relatively small particle size and highly dispersed particles at high temperature.[2] The material obtained by carbonization of Co-MOF/CTS physical mixed sample at 600 °C has slightly increased particle size (26-54 nm) and slightly decreased dispersion compared with (Co-MOF)-600 (Fig. S2e). In the particle distribution diagram of (Co-MOF/CTS)-900, compared with (Co-MOF)-900, the particle dispersion has been improved, the particle size distribution range has become smaller (111-271 nm), there is no generation of maximum particle size, and the particles can be coated by the carbon layer. In general, there is still a big gap between the control of the morphology of carbon-based materials by using physical mixed samples as precursors and Co-MOF-*g*-CTS as precursors.

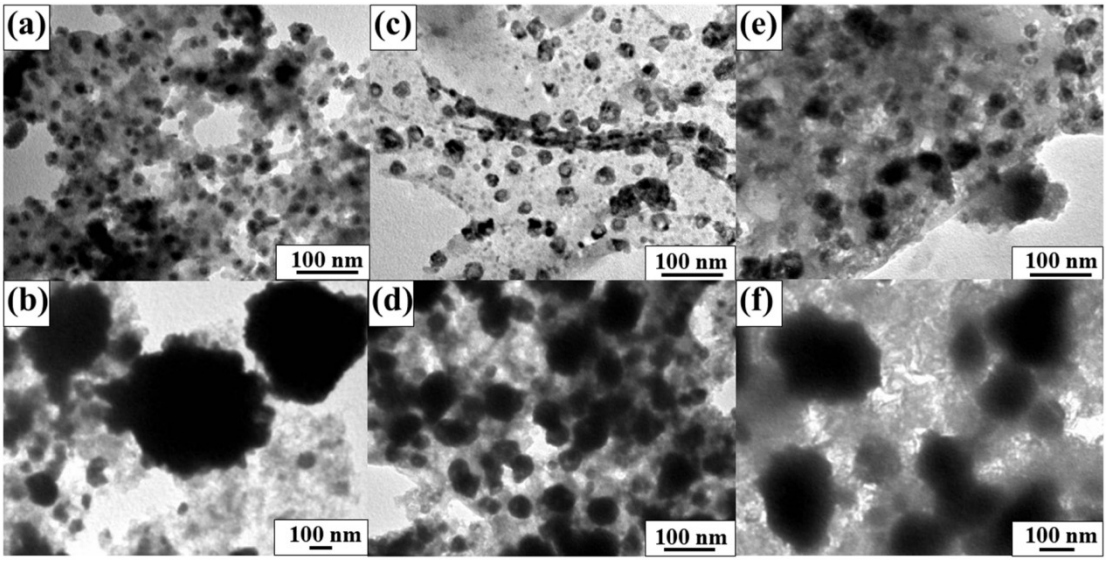

Fig. S2 TEM images of (a) (Co-MOF)-600, (b) (Co-MOF)-900, (c) (Co-MOF-*g*-CTS)-600, (d) (Co-MOF-*g*-CTS)-900, (e) (Co-MOF/CTS)-600 and (f) (Co-MOF/CTS)-900.

Due to the confinement and coating of CTS, the SEM image of (Co-MOF-*g*-CTS)-600

shows irregular small spheres with a diameter of approximately 500 nm (Fig. S3a). With the increase of the carbonization temperature(Co-MOF-g-CTS)-900 exhibits a smaller diameter of the spherical morphology and an uneven porous structure with gaps (Fig. S3b). These porous structures are conducive to the adsorption of reactants and proton transfer and play a positive role in many catalytic reactions.[3]

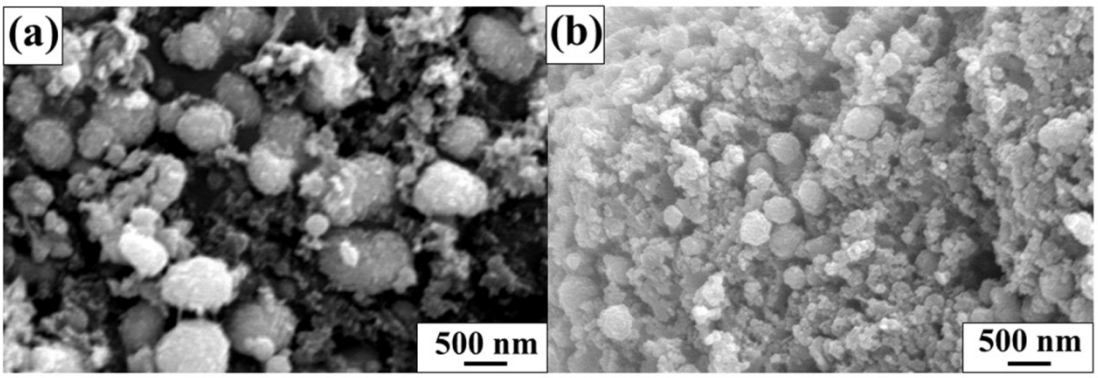

Fig. S3 SEM images of (a) (Co-MOF-*g*-CTS)-600 and (b) (Co-MOF-*g*-CTS)-900 at different scales.

As shown in Fig. S4a, the XRD curves of carbon-based materials obtained by carbonization of Co-MOF, Co-MOF-*g*-CTS and Co-MOF/CTS at 600 °C. The diffraction of (Co-MOF)-600, (Co-MOF-*g*-CTS)-600, and (Co-MOF/CTS)-600 at 44.22 ° and 51.52 ° belong to the (111) and (200) crystal planes of Co. In addition, the (Co-MOF-*g*-CTS)-600 exhibits the characteristic peak of CoO (111) plane at 36.49 °, which may be due to the existence of oxygen in CTS, leading to the formation of CoO. The flat peak near 20-25 ° is the characteristic peak of graphite carbon. Fig. S4b shows the XRD curves of carbon-based materials obtained by carbonization of Co-MOF, Co-MOF-*g*-CTS and Co-MOF/CTS at 900 °C. The characteristic peaks of (Co-MOF)-900, (Co-MOF-*g*-CTS)-900, and (Co-MOF/CTS)-900 at 44.22 ° and 51.52 ° are attributed to the (111) and (200) crystal planes of Co, and the characteristic peaks at 36.49 ° and 42.39 ° are attributed to the (111) and (200) crystal planes of CoO.[4] The diffraction peak of graphite carbon is near 20-25 °.

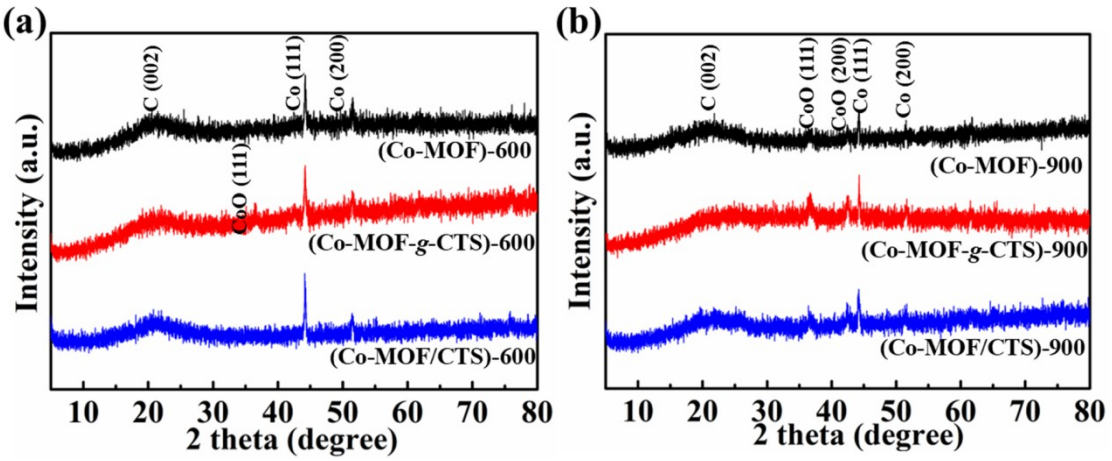

Fig. S4 XRD curves of carbon based materials obtained by carbonization of different precursors with treatments at (a) 600 °C and (b) 900 °C.

As shown in Fig. S5, (Co-MOF-*g*-CTS)-900, (Co-MOF-*g*-CTS)-900 and (Co-MOF)-900 both show typical type IV adsorption isotherms and H3 hysteresis loops. The BJH mesopore distribution showed that the pore size of (Co-MOF)-900 was concentrated around 1.75 nm, and that of (Co-MOF-*g*-CTS)-600 and (Co-MOF-*g*-CTS)-900 was about 1.90 nm. HK micropore diameter distribution showed that the micropore diameter distribution of (Co-MOF-*g*-CTS)-600 was between 0.64-1.91 nm, the micropore diameter distribution of (Co-MOF-*g*-CTS)-900 was between 0.60-2.26 nm, and the micropore diameter distribution of (Co-MOF)-900 was between 0.77-2.28 nm. (Co-MOF-*g*-CTS)-900 has larger specific surface area, larger specific pore volume and smaller pore size during pyrolysis compared with (Co-MOF-*g*-CTS)-900 and (Co-MOF)-900, which has a more positive effect on the catalytic reaction.[5]

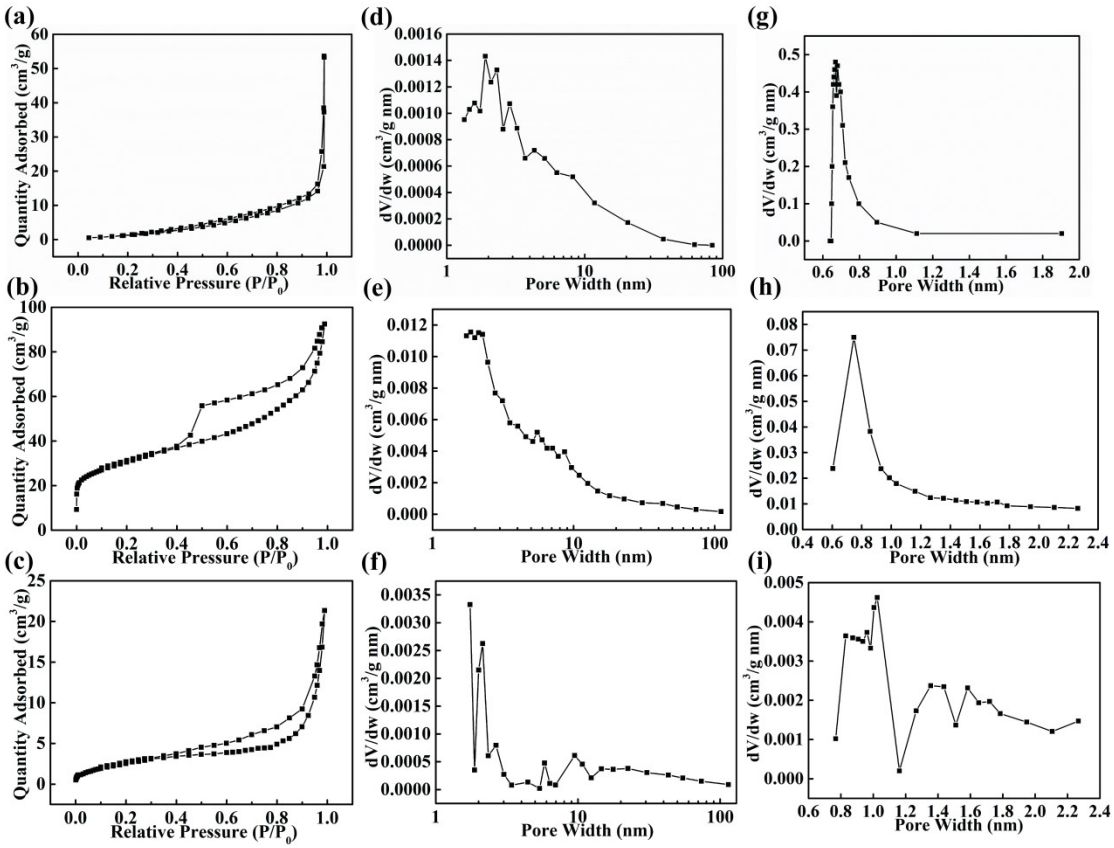

Fig. S5 N_2 adsorption desorption isotherms of (a) (Co-MOF-*g*-CTS)-600, (b) (Co-MOF-*g*-CTS)-900 and (c) (Co-MOF)-900, BJH mesoporous size distributions of (d) (Co-MOF-*g*-CTS)-600, (e) (Co-MOF-*g*-CTS)-900 and (f) (Co-MOF)-900, HK micropore size distributions of (g) (Co-MOF-*g*-CTS)-600, (h) (Co-MOF-*g*-CTS)-900 and (i) (Co-MOF)-900.

Table S2 Specific surface area, pore volume and pore diameter of (Co-MOF-*g*-CTS)-600, (Co-MOF-*g*-CTS)-900 and (Co-MOF)-900.

Sample	Specific surface area ($m^2\ g^{-1}$)	Pore volume ($cm^2\ g^{-1}$)	Aperture (nm)
(Co-MOF-*g*-CTS)-600	14	0.11	15.56
(Co-MOF-*g*-CTS)-900	103	0.14	5.58
(Co-MOF)-900	10	0.03	13.26

XPS was used to investigate the effects of different precursors and carbonization

temperatures on the states of elements in (P)-T. The four elements Co, N, C and O can be observed in the total spectrum of (Co-MOF)-600 and (Co-MOF-*g*-CTS)-900. The three elements Co, C and O can be observed in (Co-MOF)-900. In (Co-MOF-*g*-CTS)-600, the three elements N, C and O can be observed (Fig. S6a). The peaks of (Co-MOF)-600 and (Co-MOF-*g*-CTS)-900 at 777.5, 779.7, and 780.1 eV are caused by the metal Co, Co-N, and Co-O bonds.[6] (Co-MOF)-900 has only one Co-O peak at 780.1 eV and a weaker metallic Co peak at 777.5 eV, mainly due to the particles in (Co-MOF)-900 escape the carbon layer and are oxidized by oxygen in the air. Interestingly, Co2p signal was not observed at (Co-MOF-*g*-CTS)-600, because the CTS coated on the surface of Co-MOF carbonized in advance, forming a protective carbon shell that encapsulated the particle in the carbon layer (Fig. S6b). It can be seen from Fig. S6c that Co-MOF forms a Co-N bond located at 399.0 eV carbonized at 600 °C, which is an important active site for catalytic reaction.[7] However, while Co-MOF is carbonized at 900 °C, the presence of N cannot be detected by the high-resolution spectrum of N 1s, which indicates that high temperature carbonization will affect the doping of N element. (Co-MOF-*g*-CTS)-600 forms a peak of pyridine-N at 398.3 eV due to the introduction of CTS in the precursor. In the high-resolution N 1s spectrum of (Co-MOF-*g*-CTS)-900, the characteristic peak of the Co-N bond appears again, which due to the limited pyrolysis strategy protects the pyrolyzed material, and thus retains an important catalytic active site during high temperature carbonization. The peaks of (Co-MOF)-600 and (Co-MOF-*g*-CTS)-600 at 284.6 and 285.5 eV are caused by the C-C and C-N bonds, the peaks at 288.5 eV are caused by the C=O and O-C=O groups from the carboxyl group.[8] Only C-C bond (284.6eV) and weak C-N bond (285.5eV) peaks exist in (Co-MOF)-900. The peaks caused by carboxyl groups at 288.5eV completely disappear, which indicates that high temperature will completely decompose some carboxyl groups on the surface of carbon-based materials. The peaks of (Co-MOF-*g*-CTS)-900 at 284.6 and 285.5 eV are caused by the C-C and C-N bonds, and the peak strength of C-N bond is strong. High temperature heat treatment under the protection of CTS also forms the peaks of C-O and O-C=O at 286.6 and 289.1 eV (Fig. S6d).

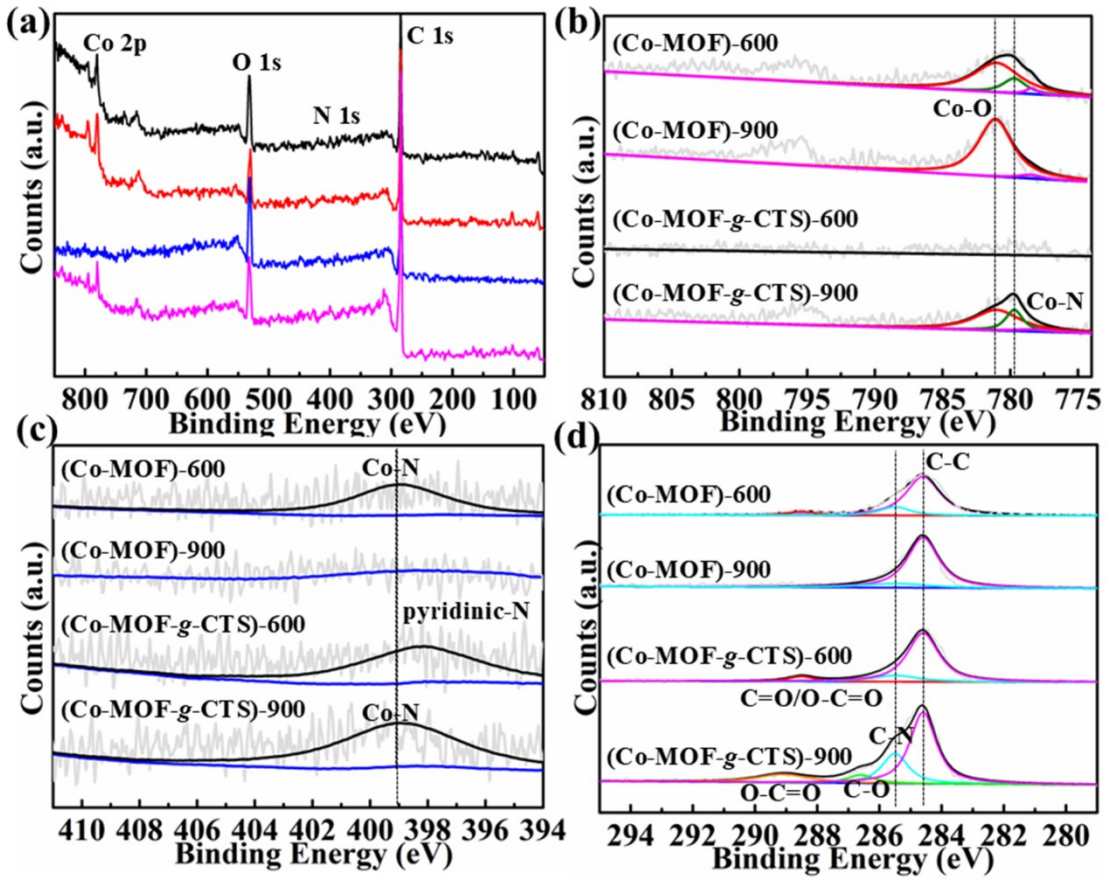

Fig. S6 XPS analysis of (Co-MOF)-600, (Co-MOF)-900, (Co-MOF-*g*-CTS)-600 and (Co-MOF-*g*-CTS)-900: (a) full spectra; High-resolution spectrum of (b) Co 2p, (c) N 1s and (d) C 1s.

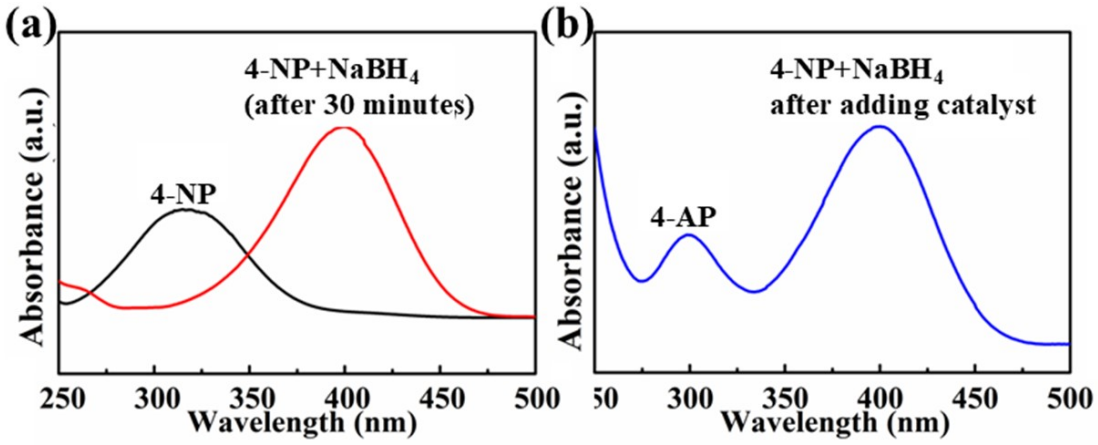

Fig. S7 (a) Characteristic absorption peak (black) of 4-NP and characteristic absorption peak (red) after adding $NaBH_4$ (30 min), (b) Characteristic absorption peak of 4-AP.

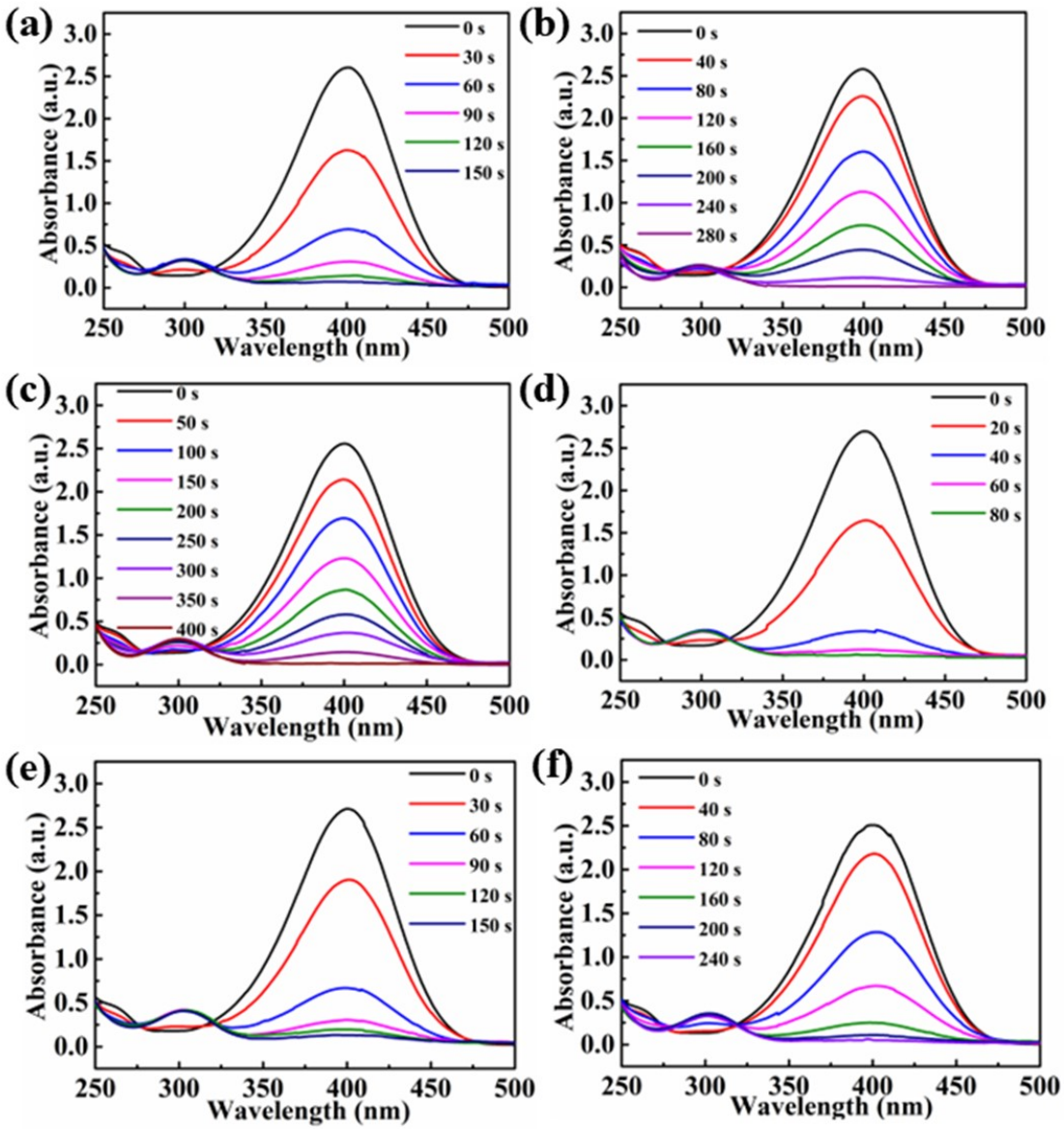

Fig. S8 UV-vis spectra of (a) (Co-MOF) -600, (b) (Co-MOF)-900, (c) (Co-MOF-*g*-CTS)-600, (d) (Co-MOF-*g*-CTS)-900, (e) (Co-MOF/CTS)-600 and (f) (Co-MOF/CTS)-900 as catalysts for catalytic reduction of 4-NP.

Table S3 Mass of catalyst in each cycle.

cycle	1	2	3	4	5
catalyst mass (mg)	0.103	0.097	0.096	0.093	0.090
cycle	6	7	8	9	10
catalyst mass (mg)	0.090	0.087	0.083	0.083	0.081

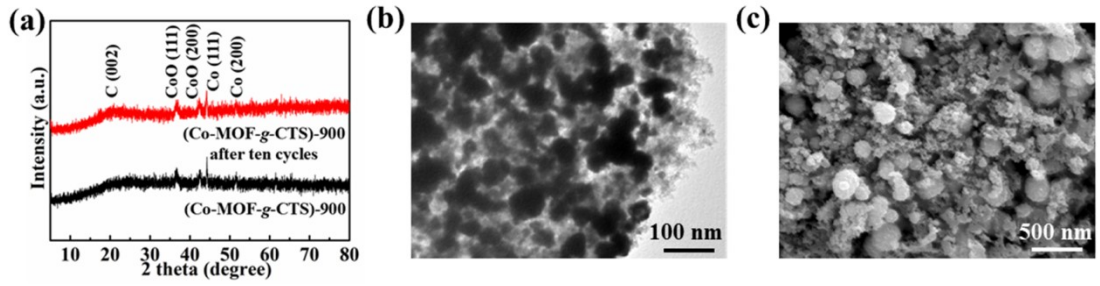

Fig. S9 (a) XRD curves of (Co-MOF-*g*-CTS)-900 after 10 cycles,

(b) TEM images and (c) SEM images of (Co-MOF-g-CTS)-900 after 10 cycles.

4. References

1. D. Xu, D. Zhang, H. Zou, L. Zhu, M. Xue, Q. Fang and S. Qiu, Chem. Commun., 2016, 52, 10513-10516.

2. M. Zhang, C. Wang, R. Luo, W. Zhang, S. Chen, X. Yan, J. Qi, X. Sun, L. Wang and J. Li, J. Mater. Chem. A, 2019,7, 5173-5178.

3. H. Zhao and L. Zhao, Dalton Trans., 2018, 47, 3321-3328.

4. X. Ma, Y.-X. Zhou, H. Liu, Y. Li and H.-L. Jiang, Chem. Commun., 2016, 52, 7719-7722.

5. D. Ding, K. Shen, X. Chen, H. Chen, J. Chen, T. Fan, R. Wu and Y. Li, ACS Catal., 2018, 8, 879-7888.

6. X. Li, C. Zeng, J. Jiang and L. Ai, J. Mater. Chem. A, 2016, 4, 7476-7482.

7. D. Wang, L. Xu, F. Zeng, X. Hu, B. Liu, C. Li, Z. Su and J. Sun, New J. Chem., 2021, 45, 13751-13754.

8. X. Liu, D. Xu, Q. Wang and L. Zhang, Small, 2018, 14, 1803188.